Sidewall boundary layer instabilities in a rapidly rotating cylinder driven by a differentially corotating lid

Juan M. Lopez[1,a)] and Francisco Marques[2,b)]
[1]*School of Mathematical and Statistical Sciences, Arizona State University, Tempe, Arizona 85287, USA*
[2]*Departament de Física Aplicada, Universitat Politècnica de Catalunya, 08034 Barcelona, Spain*

(Received 3 May 2010; accepted 12 October 2010; published online 24 November 2010)

The flow in an enclosed completely filled rapidly rotating cylinder that is driven by the differential corotation of the top lid is studied numerically. Although the flow is in a very simple geometry, the fast background rotation and large differential rotation of the lid lead to very thin boundary layers with a variety of instability modes with very fine spatial scales as well as inertial waves that are sustained in the fast rotating interior flow and that interact with the viscous modes in the sidewall boundary layer, leading to complex spatiotemporal dynamics. The numerical simulations are compared and contrasted to experimental visualizations of the sidewall boundary layer instabilities reported by Hart and Kittelman ["Instabilities of the sidewall boundary layer in a differentially driven rotating cylinder," Phys. Fluids **8**, 692 (1996)]. The experiments report observing axisymmetric rolls propagating down the sidewall layer for small differential corotation of the top lid. As the differential rotation was increased, backward tilted diagonal rolls that precess slightly retrograde with respect to the rotating sidewall and forward tilted rolls with prograde precession significantly faster than the sidewall rotation were observed. For still larger differential rotation, a wavy turbulent state that has backward tilted structures erupting from deep within the sidewall layer into the interior and is riding on the forward tilted diagonal rolls in the deep layer was observed. Our simulations capture all of these states and strongly suggest that the observed axisymmetric rolls are unstable and were only transiently observed due to the slow and continuous increase in the differential rotation employed in the experiments. The influence of inertial waves driven by the sidewall instabilities on the three-dimensional wavy turbulent state is discussed. © *2010 American Institute of Physics*. [doi:10.1063/1.3517292]

I. INTRODUCTION

Confined rapidly rotating flow subjected to differential rotation of the container has attracted much attention. These flows are of practical importance in many areas, such as rotating machinery[1,2] and models of wind-driven ocean circulations.[3–6] In the latter models, laminar flow and sidewall boundary layer stability to small scale disturbances are usually assumed. More recent interest in this class of problems comes from laboratory models used to study the structure of vertical boundary layers in differentially rotating systems and other processes in geophysical systems. Hart and Kittelman[7] considered the flow in a rotating cylinder that is driven by the differential rotation of the top endwall. They observed a number of waves (both axisymmetric rolls and diagonal rolls inclined to the axis) that appear in the sidewall boundary layer region when the top endwall is rotating sufficiently faster than the sidewall. They presented tentative physical arguments to explain the origin of these instabilities. However, there is a lack of knowledge concerning even the structure of the basic state of this differentially rotating system from which to study its stability.

The analysis of Stewartson[8] is a classical treatment of a very closely related problem, where the sidewall of a cylinder rotates differentially to its top and bottom endwalls (Stewartson's "second" problem, the "first" being the split-disk flow). The analytical description of the multilayered structure of the sidewall boundary layer required a number of approximations to the governing equations to reach a tractable analytic problem, beginning with the restriction to very small differential rotation so that the nonlinear terms could be neglected and appealing to the thinness of the boundary layer to justify neglect of the curvature effects. Under these conditions, Stewartson was able to show that the shear flow that forms near the sidewall has a two-layered structure with the outer layer being essentially height-invariant, whereas the inner layer varies with the distance along the sidewall.

Efforts to study the stability of Stewartson boundary layers on cylinder walls have not been able to capture the experimentally observed instability modes; those studies made assumptions that are incompatible with the observations: assuming that the instability mode would be stationary, axisymmetric, and periodic in the axial direction.[9] While some of the observed instability modes are axisymmetric, they are not stationary nor axially periodic, consisting instead of axially propagating rolls.[7]

An early description of the basic states in differentially rotating cylinders, based on numerical solutions of the axisymmetric Navier–Stokes equations, was presented by Lopez,[10] who also reported an unsteady axisymmetric instability of the sidewall boundary layer consisting of propagat-

[a)]Electronic mail: lopez@math.asu.edu.
[b)]Electronic mail: marques@fa.upc.edu.

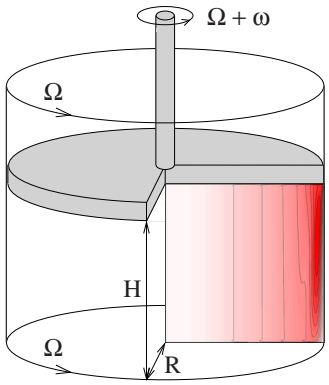

FIG. 1. (Color online) Schematic of the apparatus including streamlines of a basic state at $\mathrm{Re}=4.4\times10^4$, $\mathrm{Ro}=0.46$, and $\gamma=1$. The contours are equispaced; the dark (red) shades are positive values and the light (blue) shades are negative, with zero being white.

ing waves localized near the bottom corner. These have a character very different from the axisymmetric propagating waves observed in the experiments of Hart and Kittelman,[7] which were localized closer to the top corner where the strong radial flow in the top Ekman layer is turned into the sidewall layer. This apparent discrepancy is resolved in this study, where we have identified two distinct axisymmetric wave modes of instability that are prominent in different parameter regimes, and we have located where in parameter space they compete directly. The experiments also report nonaxisymmetric modes, and we also capture these in the simulations presented in this paper.

II. GOVERNING EQUATIONS AND NUMERICAL METHODS

Consider the flow in a circular cylinder of radius R and height H completely filled with a fluid of kinematic viscosity ν. The cylinder sidewall and bottom endwall rotate with angular speed Ω, while the top endwall has a differential rotation of angular speed $\Omega+\omega$. A schematic of the flow system is shown in Fig. 1. The Navier–Stokes equations, nondimensionalized using R as the length scale and $1/\Omega$ as the time scale, are

$$(\partial_t+\mathbf{u}\cdot\nabla)\mathbf{u}=-\nabla p+\frac{1}{\mathrm{Re}}\nabla^2\mathbf{u},\quad \nabla\cdot\mathbf{u}=0, \tag{1}$$

where $\mathbf{u}=(u,v,w)$ is the velocity field in polar coordinates $(r,\theta,z)\in[0,1]\times[0,2\pi]\times[0,\gamma]$, the vorticity is $\nabla\times\mathbf{u}=(\xi,\eta,\zeta)=[1/r\partial_\theta w-\partial_z v,\partial_z u-\partial_r w,1/r\partial_r(rv)-1/r\partial_\theta u]$, and p is the kinematic pressure. The following are the three governing parameters:

$$\text{Reynolds number: } \mathrm{Re}=\Omega R^2/\nu,$$

$$\text{Rossby number: } \mathrm{Ro}=\omega/\Omega,$$

$$\text{aspect ratio: } \gamma=H/R.$$

In these types of problems, an Ekman number is often used instead of the Reynolds number; these two are related as $E=\nu/(2\Omega H^2)=1/(2\gamma^2\ \mathrm{Re})$. The Rossby number (Ro) is a measure of the differential rotation. In presenting their experimental results, Hart and Kittelman[7] defined the Rossby number as $\mathrm{Ro}^H=(\omega R)/(\Omega L_S)$, where $L_S=\nu/(2\Omega)^{1/4}H^{1/2}=HE^{1/4}$ is an estimate of the sidewall boundary layer thickness. The relationship between the two Rossby numbers is $\mathrm{Ro}=\omega/\Omega=2\gamma E^{1/4}\ \mathrm{Ro}^H$. For numerical implementation, it is much more straightforward to use Re and Ro.

The boundary conditions are no-slip: on the rotating cylinder sidewall $(u,v,w)=(0,1,0)$, on the differentially rotating top endwall $(u,v,w)=[0,r(1+\mathrm{Ro}),0]$, and on the rotating bottom endwall $(u,v,w)=(0,r,0)$. The idealized boundary conditions are discontinuous at the junction where the rotating cylinder meets the differentially rotating top endwall at $(r=1,z=\gamma)$. In a physical experiment, there is a small but finite gap at this junction where the azimuthal velocity adjusts rapidly between 1 and $1+\mathrm{Ro}$. For an accurate use of the spectral techniques, a regularization of this discontinuity is implemented in the form

$$v(r,\theta,\gamma,t)=r(1+\mathrm{Ro}\{1-\exp[(r-1)/\epsilon]\}), \tag{2}$$

where ϵ is a small parameter that mimics the small physical gap (we have used $\epsilon=0.003$). The use of $\epsilon\neq0$ regularizes the otherwise discontinuous boundary condition (see Ref. 11 for further details on the use of this technique in the spectral codes).

The governing equation (1) has been solved using a second-order time-splitting method, with space discretized via a Galerkin–Fourier expansion in θ and Chebyshev collocation in r and z. The spectral solver is based on that described in Ref. 12 and it has recently been tested and used in a wide variety of enclosed cylinder flows.[13–16] For the solutions presented here, with $\gamma=1$, we have used up to $n_r=n_z=96$ Chebyshev modes in the radial and axial directions and up to $n_\theta=392$ azimuthal Fourier modes, depending on Re, Ro, and the azimuthal wavenumber of the computed solutions, leading to a system with about 1.4×10^7 degrees of freedom. This problem requires such high spectral resolution because of the high Reynolds numbers involved, $\mathrm{Re}\sim5\times10^4$, and the very thin boundary layers where the dynamics is concentrated. Time steps $\delta t=2\times10^{-3}$ have been required for numerical stability and accuracy of the second-order temporal scheme for the axisymmetric simulations, and for the three-dimensional cases, $\delta t=7.5\times10^{-4}$ was needed with $n_\theta=392$. The viscous time in this problem is Re, although at the high Re involved, this is not the relevant time scale, and the transients and dynamics tend to evolve on a much shorter time scale $\mathrm{Re}^{1/2}$; our simulations have been run out to about 10 or 20 times $\mathrm{Re}^{1/2}$.

In reporting the axisymmetric results, we have made use of the stream function ψ, which satisfies $u=-(1/r)\partial\psi/\partial z$ and $w=(1/r)\partial\psi/\partial r$, and the azimuthal component of vorticity η as usual. We have also used the vertical vorticity ζ. Note that while ψ and η are independent of the rotating frame of reference, ζ is not, and since there is no distinguished rotating frame due to the differential rotation of the problem, we compute and present results in the inertial (i.e., stationary) frame of reference.

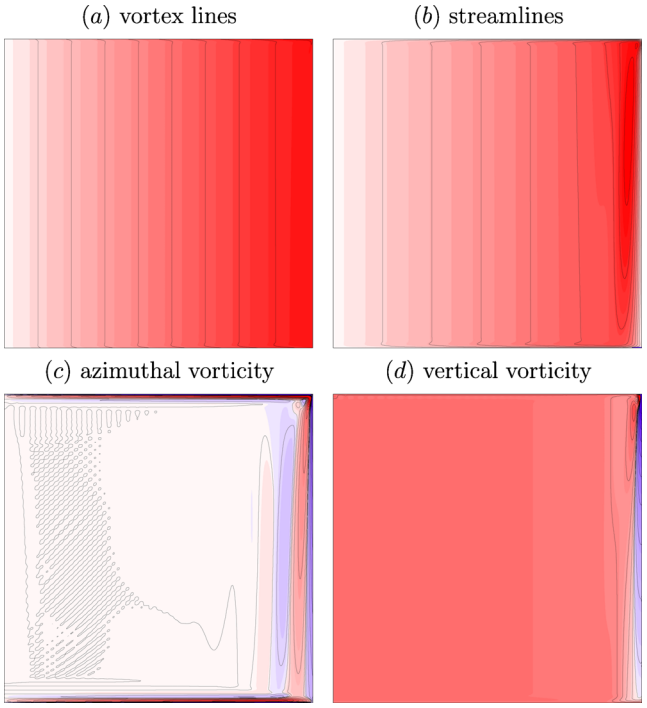

FIG. 2. (Color online) A basic state at $\mathrm{Re}=5\times10^4$, Ro=0.40, and $\gamma=1$ showing the vortex lines rv, the streamlines ψ, the azimuthal vorticity η, and the vertical vorticity ζ. The contours are quadratically spaced in the ranges $rv\in[0,1.4]$, $\psi\in[0,10^{-3}]$, $\eta\in[-10,10]$, and $\zeta\in[-10,10]$; the dark (red) shades are positive values and the light (blue) shades are negative, with zero being white.

III. STEADY, AXISYMMETRIC BASIC STATE

A typical basic state at $\mathrm{Re}=5\times10^4$ and Ro=0.40 for $\gamma=1$ shown in Fig. 2 illustrates the salient features from the analysis of these types of flows that Stewartson[8] first presented. The vortex lines [contours of rv, presented in part (a) of the figure] show the bulk flow to be very close to solid-body rotation with a rotation speed intermediate between that of the top and bottom endwalls, as predicted by Stewartson[17] for the flow between two rotating disks of infinite radius. In the radially unbounded problem, the (nondimensional) vertical vorticity of the bulk flow between the disks would be $\zeta=2+\mathrm{Ro}$, independent of r and z. The presence of the sidewall introduces a very weak dependence on r outside the sidewall boundary layer (in this example, for $r\lesssim0.8$). Figure 3 shows how ζ, measured at a point $(r,z)=(0.4,0.5)$ for

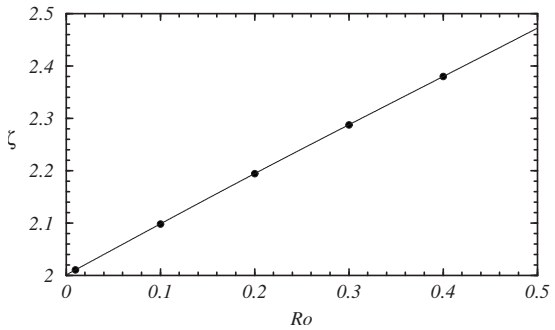

FIG. 3. Vertical vorticity at a point $(r,z)=(0.4,0.5)$ in the bulk of the flow as a function of Ro for $\mathrm{Re}=5\times10^4$, $\gamma=1$.

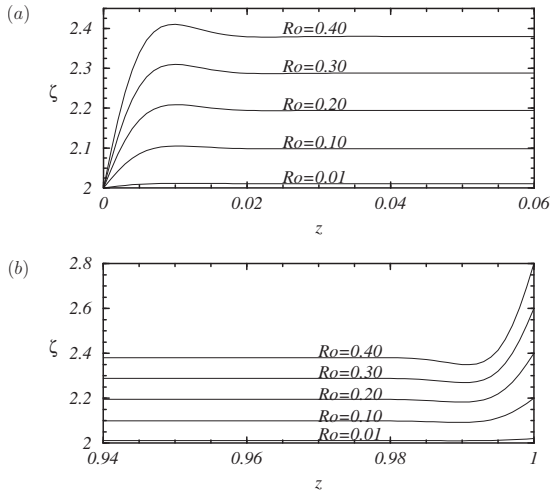

FIG. 4. Vertical profiles of the vertical vorticity, ζ, at $r=0.4$ for $\mathrm{Re}=5\times10^4$, $\gamma=1$ and Ro as indicated, near (a) the bottom endwall and (b) the top endwall.

$\mathrm{Re}=5\times10^4$ and $\gamma=1$, varies with Ro; the dependence is, as expected, linear with a slope slightly less than the theoretical value for unbounded disks of infinite radius. The boundary layers on the bottom and top endwalls are also very much as one would expect from similarity solutions for unbounded rotating disk flows (see Fig. 4).

The quasigeostrophic bulk flow (essentially independent of z, except in the top and bottom boundary layer regions) extends out to about $r=0.8$, where the influence of the sidewall layer begins to be non-negligible. The azimuthal vorticity contours [Fig. 2(c)] highlight the radial extent of the sidewall layer as well as its radially oscillatory nature. The streamline plot [Fig. 2(b)] shows that the sidewall boundary layer flow has z-dependence, particularly near the top and bottom corners, and that the flow in the region nearest the wall flows down the wall rapidly, as expected due to the flow driven from the top Ekman layer. The Ekman layer on the top, which forms as a result of the differential rotation, drives a relatively strong meridional circulation that is confined to the region near the sidewall; the streamlines show that there is a strong upward flow immediately adjacent in the outer boundary layer region. These two regions are distinguished more readily by the vertical vorticity, which is strongly negative in the inner region closest to the wall with downward-directed flow, while in the outer region with upward-directed flow, the vertical vorticity is positive and overshoots that of the bulk flow in near solid-body rotation [Fig. 2(d)].

Radial profiles of the vertical vorticity at heights $z=0.1i$, $i=1\rightarrow9$, for $\mathrm{Re}=5\times10^4$, $\gamma=1$, and Ro=0.1, 0.2, and 0.4 are shown in Fig. 5; only the parts of the profiles near the sidewall are shown as they rapidly asymptote toward the unbounded disk constant limit of $\zeta=2+\mathrm{Ro}$ as r decreases from about 0.8. Their approach toward the wall $(r\rightarrow1)$ is not monotonic, and for $\mathrm{Ro}\gtrsim0.2$, the vertical vorticity first overshoots above the bulk flow value, and then as it approaches the wall, it becomes very negative. This behavior is most prominent near the top corner. These large overshoots, in the positive and negative directions, in the vertical

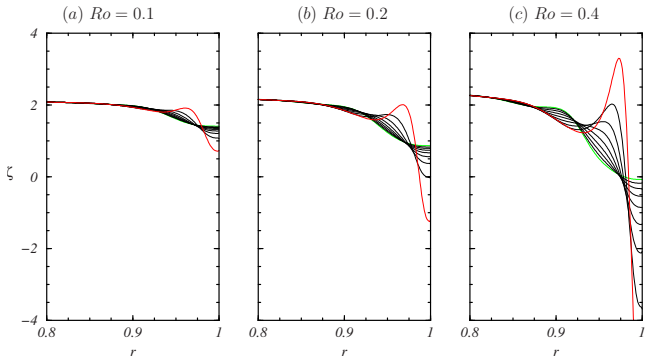

FIG. 5. (Color online) Radial profiles of the vertical vorticity ζ for Re=5×10^4, γ=1, and Ro, as indicated, at nine equispaced axial locations in $z\in[0.1,0.9]$. The profiles with the largest overshoots near the wall, r=1, correspond to the largest z; the z=0.9 profile is red and the z=0.1 profile is green.

vorticity result in a sidewall boundary layer that is very inflectional and thus susceptible to instability. We note that Hart and Kittelman[7] considered shear layer instability as a possible cause of some of the instability modes they observed, but were concerned that "the fundamental Stewartson boundary layer solution has no inflection points."

Figure 6 shows the radial profiles of the azimuthal velocity in a frame of reference rotating with the sidewall and bottom, $v-r$. Part (a) of the figure shows the profiles at height z=0.9, near the top, of the basic states at Re=5×10^4 and γ=1 for various Ro. In all cases, as indicated earlier, the flow in the bulk rotates as a solid body, out to about r=0.8, at a rate half way between that of the top and bottom endwalls. For very small Ro$\sim$0.01, the profiles in the boundary layer monotonically reduce to zero at the wall. As Ro is increased, the profiles in the layer developed inflection points of the type consistent with inviscid instability according to Fjortoft's[18,19] necessary condition for inviscid instability. Part (b) of the figure is a close-up of these profiles in the boundary layer region $r\in[0.8,1.0]$. The inflectional nature of the boundary layer is most pronounced near the top

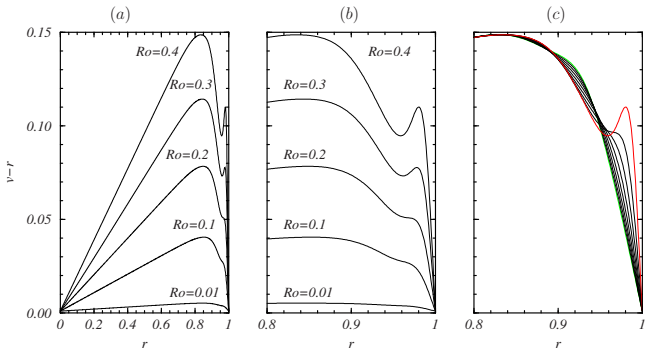

FIG. 6. (Color online) Radial profiles of the relative azimuthal velocity, $v-r$, for Re=5×10^4, γ=1, and Ro, as indicated, at height z=0.9; (a) shows the profiles over the whole radius and (b) is a close-up of these near the wall; (c) are the profiles for Ro=0.4 at nine equispaced axial locations in $z\in[0.1,0.9]$. The profiles with the largest overshoots near the wall, r=1, correspond to the largest z; the z=0.9 profile is red and the z=0.1 profile is green.

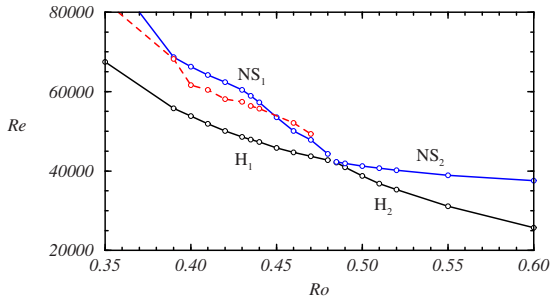

FIG. 7. (Color online) Regime diagram in the (Re,Ro) space showing the two axisymmetric Hopf bifurcation curves, H_1 and H_2 (black), as well as Neimark–Sacker curves, NS_1 and NS_2 (blue), and the curve (red dashes) above which temporally complex flows appear.

endwall. In part (c) of the figure, profiles for the Ro=0.4 case at heights $z=0.1i$, $i=1\rightarrow9$, are shown. By $z\approx0.7$, the boundary layer has lost its inflectional nature.

IV. AXISYMMETRIC INSTABILITIES OF THE SIDEWALL LAYER

Before conducting three-dimensional simulations, which are very demanding due to the high Reynolds numbers involved, we have investigated the axisymmetric flow extensively, determining its stability and nonlinear dynamics. The regime diagram (Fig. 7) shows two Hopf bifurcation curves, labeled H_1 and H_2, in the (Re,Ro) parameter space. Below these two curves, the steady basic state, as described in Sec. III, is stable to axisymmetric perturbations, and upon crossing these curves, the basic state loses stability via supercritical Hopf bifurcations and limit cycle solutions are born, LC_1 upon crossing H_1 and LC_2 upon crossing H_2.

The LC_1 periodic state consists of rolls that form essentially on about the inflection point in the upper half of the sidewall layer, and these rolls propagate down the sidewall layer and die out as the inflectional nature of the sidewall layer diminishes with distance down from the top corner. The instability is localized in the inner layer. This state has many characteristics that are in common with the axisymmetric roll state observed by Hart and Kittelman;[7] they provided a photograph in their Fig. 2(a) at $\sqrt{E}=2.17\times10^{-3}$, $\mathrm{Ro}^H=2.0$, and γ=1.16 (in terms of the parameters used in this study, Re=7.9×10^4 and Ro=0.216). The outer layer, the Ekman layers on the top and bottom endwalls and the bulk flow, all remain essentially steady and virtually indistinguishable from those of the basic state; compare the basic state azimuthal vorticity at $(\mathrm{Ro},\mathrm{Re})=(0.40,5.0\times10^4)$, shown in Fig. 2(c), with that of LC_1 at the same Re and slightly larger Ro=0.45, shown in Fig. 8(a). The zero contour level meanders all over the interior bulk flow region, indicating that the flow there essentially has no meridional component (i.e., $u=w=0$). The accompanying movie available with the online version shows the LC_1 state over several oscillation cycles, illustrating its dynamics.

The nature of LC_2 is quite different to that of LC_1. Apart from having the roll oscillations located at the bottom half of the sidewall layer and reaching maximum amplitude at the bottom corner, as is evident in the snapshot of LC_2 azimuthal

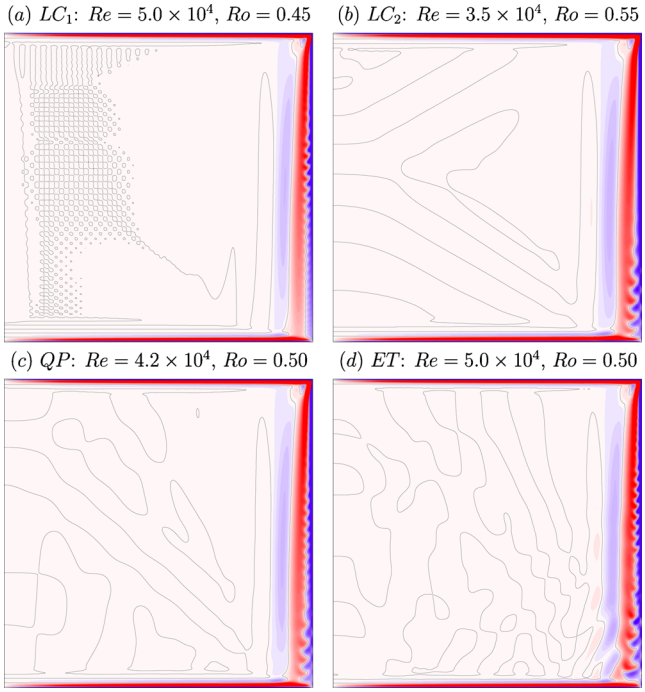

FIG. 8. (Color online) Snapshots of η for (a) LC_1 at Re=5.0×10^4, Ro=0.45; (b) LC_2 at Re=3.5×10^4, Ro=0.55; (c) QP at Re=4.2×10^4, Ro=0.50; and (d) ET at Re=5.0×10^4, Ro=0.50, all with $\Gamma=1$. The black contour is the zero contour and the color map is for $\eta\in[-2,2]$ with blue negative, white zero, and red positive. Note that min $\eta\approx-90$ and max $\eta\approx20$, but these occur very localized near the top corner (enhanced online) [URL: http://dx.doi.org/10.1063/1.3517292.1] [URL: http://dx.doi.org/10.1063/1.3517292.2] [URL: http://dx.doi.org/10.1063/1.3517292.3] [URL: http://dx.doi.org/10.1063/1.3517292.4].

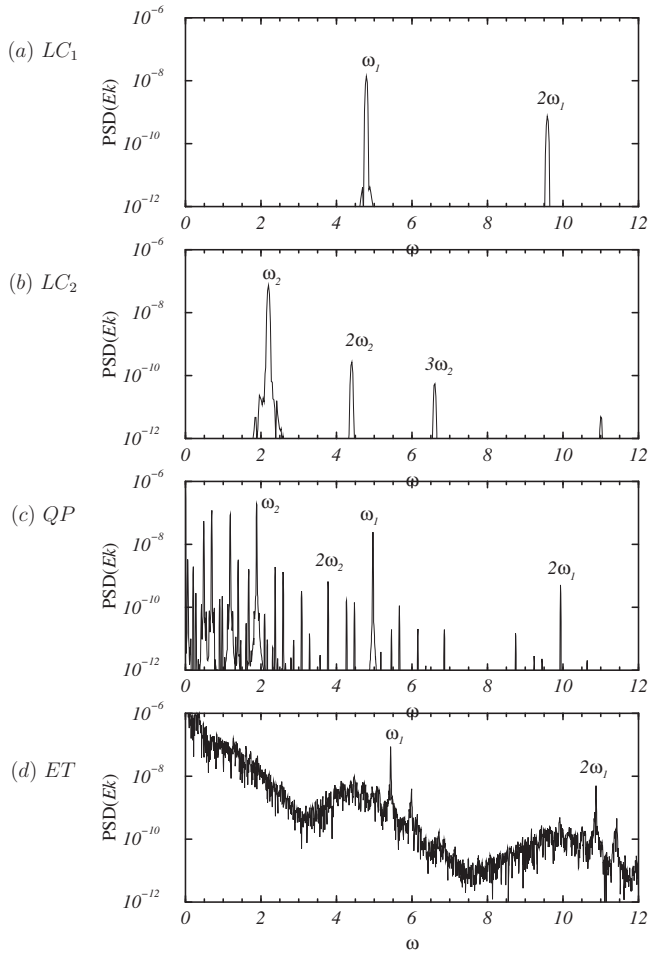

FIG. 9. Power spectral densities of Ek for the four states shown in Fig. 8.

vorticity shown in Fig. 8(b), the unsteadiness is no longer confined to the inner layer. The associated online movie shows oscillations in the Ekman layer at the bottom disk near the sidewall, as well as disturbances propagating upward along the interface between the quasigeostrophic bulk and the outer layer, at about $r=0.8$. The LC_2 state is the unsteady axisymmetric state reported by Lopez[10] at Re=6×10^4, Ro=0.5, and $\gamma=0.5$.

Apart from the difference in z-locations where the waves associated with LC_1 and LC_2 are found, these limit cycles are also distinguished by their frequencies. These frequencies depend on Ro and to a lesser degree on Re. The frequency of LC_1 varies from $\omega_1\approx3.3$ for Ro=0.3 to $\omega_1\approx8.2$ for Ro=0.48, whereas the frequency of LC_2 varies from $\omega_2\approx1.6$ for Ro=4.85 to $\omega_2\approx2.2$ for Ro=0.6. Figures 9(a) and 9(b) show the power spectral densities (PSDs) of the kinetic energy, Ek, of the LC_1 and LC_2 states in Fig. 8, where $Ek=2\pi\int_0^\gamma\int_0^1(u^2+v^2+w^2)\mathrm{d}r\mathrm{d}z$. The PSD clearly shows these states to be periodic, LC_1 with frequency $\omega_1\approx4.8$ and for LC_2, $\omega_2\approx2.2$. The difference in the frequencies of the two states is a significant factor in how the waves in the sidewall boundary layer interact (or not) with the bulk flow. The inviscid theory of unbounded rotating flow[20] states that inertial waves only exist for frequencies from zero to twice the rotation rate of the fluid (for our problem, the nondimensional rotation rate of the bulk is $1+\mathrm{Ro}/2$), and the angle the inertial waves travel at is related to the frequency (from traveling perpendicular to the axis for zero frequency, to traveling parallel to the axis for the maximum frequency). From the online movies associated with Figs. 8(a) and 8(b), it is evident that LC_1 does not excite inertial waves in the bulk, whereas inertial waves are generated by LC_2; their frequencies being consistent with the constraints from the inviscid theory. For the state shown in Fig. 8(b) with $\omega_2\approx2.2$, the inviscid theory states that it should propagate at an angle to the rotation axis $\theta_{\mathrm{wave}}=\cos^{-1}[\omega_2/(1+\mathrm{Ro}/2)]\approx30°$, which is approximately the angle it travels at as it emerges out of the boundary layer on the lower endwall. We shall see in later sections that viscous and nonlinear effects in the boundary layers interact with the inertial modes and this interaction plays a central role in the transition to complex flow.

At point $(\mathrm{Ro},\mathrm{Re})=(0.482,4.25\times10^4)$, the two Hopf bifurcation curves cross each other; the intersection point is a codimension-2 double Hopf bifurcation point. Figure 7 only shows the parts of H_1 and H_2 either side of their intersection point that can be determined directly by extrapolating the amplitudes of the limit cycles to zero as the curves are approach from above. The other parts of the Hopf curves are not directly observable, as upon crossing them, the basic state, already unstable to one limit cycle, undergoes another Hopf bifurcation spawning the other limit cycle, but it emerges unstable and hence is not directly observable. Associated with double Hopf bifurcations are two other bifurca-

tion curves of Neimark–Sacker type, NS_1 and NS_2. Upon crossing each one of these, one of the two coexisting limit cycles changes its stability type and a mixed mode (a quasiperiodic state inheriting the two frequencies of the two limit cycles) is spawned. Depending on which limit cycle changes its stability type, the mixed mode is either stable or unstable.[21,22] We have encountered and analyzed double Hopf bifurcations in a variety of rotating flows where the mixed mode was either unstable[23–26] or stable.[27] In this particular problem, the mixed mode is stable.

Stable LC_2 states only exist between the curves H_2 and NS_2 in Fig. 7, and for this region, $\mathrm{Re} < 4.25 \times 10^4$. In their "large tank" with $\gamma = 1.16$, the largest Ekman number that Hart and Kittelman[7] reported is $\sqrt{E} \approx 0.0027$, which corresponds to $\mathrm{Re} \approx 5 \times 10^4$; this is close to a lower bound in Re for the operation of their apparatus, and so LC_2 states were inaccessible in their experiments.

A snapshot of the mixed mode, QP, is shown in Fig. 7(c), and an animation illustrating its spatiotemporal characteristics is available online. The state shown is for $\mathrm{Re} = 4.2 \times 10^4$ and $\mathrm{Ro} = 0.50$, which is quite close to the double Hopf point. It is observed that the mixed mode consists of LC_1 waves in the upper part of the sidewall layer superimposed on LC_2 waves in the lower part, with little interaction between them. The PSD of Ek for this flow [Fig. 9(c)] consists of peaks at the two corresponding frequencies, ω_1 and ω_2, plus their linear combinations. The characteristics of the inertial waves in the bulk are somewhat changed, presumably due to the additional lower frequencies introduced by some linear combinations of ω_1 and ω_2.

Further away from the Hopf and Neimark–Sacker curves, we also find states ET with more erratic temporal behavior, but their spatial characteristics are very similar to the mixed mode QP. An example of such a state is presented in Fig. 8(d) and the accompanying online movie, at $\mathrm{Re} = 5 \times 10^4$ and $\mathrm{Ro} = 0.50$. The waves in the sidewall layer associated with LC_1 and LC_2 are still clearly evident, but unlike the QP state, for this ET state, the two wave types are interacting nonlinearly and the temporal spectra are much more broadband. Figure 9(d) gives the PSD of the corresponding Ek; there is a clear signal of the LC_1 wave, but the frequency peak of the LC_2 wave component, which is evident in the movies, is completely swamped in the broadband spectrum at the lower frequencies.

The ET states for $\mathrm{Ro} \gtrsim 0.46$ appear to emerge smoothly from the QP state, but they have been found to coexist with QP over regions of parameter space close to NS_1 and a little removed from the double Hopf point. While these erratic states are not likely to be directly associated with the double Hopf bifurcation, we note that the Neimark–Sacker bifurcation NS_1 becomes subcritical for $\mathrm{Ro} \lesssim 0.46$. Near the curve NS_1, both LC_1 and QP are found to be stable; stable LC_1 states can be computed up to the NS_1 curve, and stable QP states have been found below the curve.

We have not investigated these nonperiodic axisymmetric states any further, as at this point, it is necessary to address whether these axisymmetric states are robust to general three-dimensional perturbations. We remind the reader that all of the results presented so far have been found by restricting the computations to the axisymmetric Navier–Stokes equations.

V. THREE-DIMENSIONAL FLOWS

The three-dimensional simulations for this problem are very challenging due to the very large azimuthal wavenumbers involved, and so only a few representative cases in the neighborhood of the axisymmetric double Hopf bifurcation are presented. If we are sufficiently below the two Hopf bifurcation curves in the (Re,Ro) parameter space, the axisymmetric solutions are stable; direct numerical simulations starting with the axisymmetric state to which small random perturbations are introduced to all nonaxisymmetric Fourier components (of the order of 10^{-10} times the magnitude of the axisymmetric flow) evolve back toward the basic state. However, for cases studied above the Hopf curves, the flow does not settle onto any axisymmetric state. In particular, we have not been able to reproduce either of the axisymmetric roll solutions (LC_1 and LC_2) in a full three-dimensional simulation, at least not in the small parameter regime investigated near the double Hopf point. At this point, it is worthwhile reviewing some of the experimental observations and how they were obtained in order to put into perspective the three-dimensional results.

An important factor in the experimental technique is the use of a slow ramp in parameters to quasistatically explore a large range of parameter space in a reasonable time. Hart and Kittelman[7] started the system in solid-body rotation at some fixed Re and then slowly increased the differential rotation of the lid, Ro, over "several hours" and recorded the sidewall layer on video using Kalliroscope for the flow visualization. This slow ramping in Ro is presumed to be quasistatic, so the instantaneous state of the flow during the ramp-up is assumed to correspond to the time-asymptotic state at the corresponding Ro. The viscous time in those experiments is $R^2/\nu \approx 17$ h ($R \approx 26$ cm is the cylinder radius, $H \approx 22.4$ cm is the cylinder height, and the working fluid was water with kinematic viscosity $\nu \approx 0.01$ cm^2/s), and so the total run times over which Ro is continuously ramped are somewhat less than a viscous time. Ramping up of the differential rotation, Ro, provides an axisymmetric forcing since the basic state varies with Ro. Apart from small imperfection effects, the ramping does not provide nonaxisymmetric forcing, and so three-dimensional perturbations are damped until Ro has been ramped past its critical value for the onset of three-dimensional instabilities. However, since the experiments are started at a low Ro where all three-dimensional perturbations are damped, the initial growth of three-dimensional perturbations is from a very small level, whereas the axisymmetric perturbations are always large as any change in Ro is a direct perturbation to the basic state. Hence, it is to be expected that three-dimensional perturbations may not grow to nonlinearly saturate before Ro has been ramped to values where the axisymmetric rolls appear, even if the flow for fixed values of the parameters is unstable to three-dimensional perturbations at Ro smaller than that for the axisymmetric roll waves. This is a plausible explanation of why the axisymmetric rolls are observed in the experi-

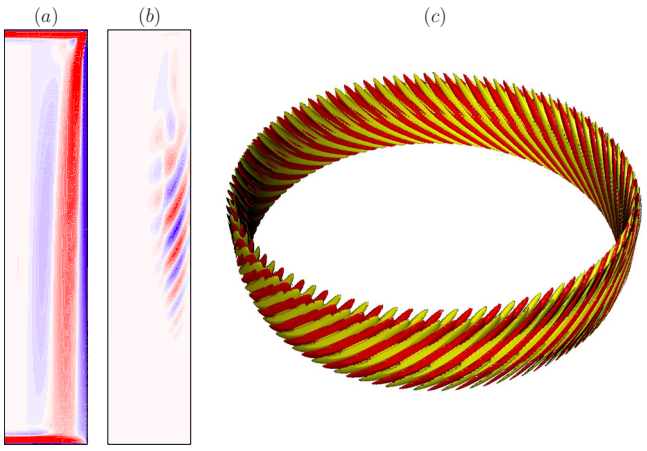

FIG. 10. (Color online) Snapshots of azimuthal vorticity η for the state at $\mathrm{Re}=3.2\times10^4$ and $\mathrm{Ro}=0.50$: contours in a partial plane $(r,z)\in[0.8,1.0]\times[0.0,1.0]$ for (a) $\eta\in[-2.0,2.0]$ and (b) $(\eta-\eta_0)\in[-0.02,0.02]$, where positive levels are red (light), negative levels are blue (dark), and zero is white, and (c) isosurfaces of $(\eta-\eta_0)$, the red (dark) isosurfaces are at level 0.01 and the yellow (light) isosurfaces are at level -0.01 (enhanced online) [URL: http://dx.doi.org/10.1063/1.3517292.5] [URL: http://dx.doi.org/10.1063/1.3517292.6] [URL: http://dx.doi.org/10.1063/1.3517292.7].

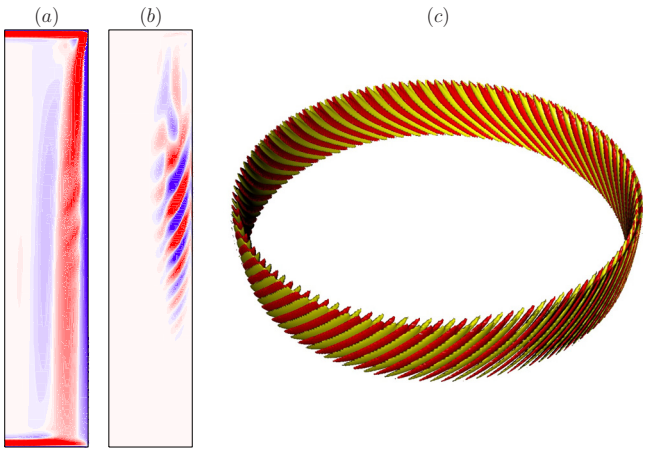

FIG. 11. (Color online) Snapshots of azimuthal vorticity η for the state at $\mathrm{Re}=3.5\times10^4$ and $\mathrm{Ro}=0.50$: contours in a partial plane $(r,z)\in[0.8,1.0]\times[0.0,1.0]$ for (a) $\eta\in[-2.0,2.0]$ and (b) $(\eta-\eta_0)\in[-0.2,0.2]$, where positive levels are red (light), negative levels are blue (dark), and zero is white, and (c) isosurfaces of $(\eta-\eta_0)$, the red (dark) isosurfaces are at level 0.1 and the yellow (light) isosurfaces are at level -0.1.

ments even though the numerical simulations suggest that they are unstable to three-dimensional perturbations.

The first nonaxisymmetric state observed experimentally as Ro is ramped is described as consisting of stationary nonpropagating rolls that are tilted backward with height. By stationary nonpropagating, Hart and Kittelman[7] meant that these tilted rolls are corotating with the sidewall, and since their videos are taken in the rotating frame, they appear to be stationary. This raises the issue that since axisymmetry [(SO(2) symmetry] is being broken, the resulting pattern should generically precess.[28,29] Of course, it could happen that the pattern precession exactly coincides with the wall rotation, but generically this would only occur at a particular value of Ro, not over a range of Ro as reported. Possible explanations for this could be that the pattern is not exactly stationary relative to the wall, or that there are small imperfections in the apparatus to which the otherwise slowly precessing pattern is pinned. We have found these backward tilted roll solutions for parameter values slightly below the two Hopf curves in Fig. 7, and they have a very slight retrograde precession relative to the sidewall. Two such examples are shown in Figs. 10 and 11, both at $\mathrm{Ro}=0.50$ with $\mathrm{Re}=3.2\times10^4$ and $\mathrm{Re}=3.5\times10^4$, respectively. The figures show contours of the azimuthal vorticity η near the sidewall, $(r,z)\in[0.8,1]\times[0,1]$, as well as the nonaxisymmetric components, $(\eta-\eta_0)$, where η_0 is the axisymmetric component of η. The structure of $(\eta-\eta_0)$ provides a good estimate of the structure of the η eigenmode. The third panel in the figures shows two isosurfaces of $(\eta-\eta_0)$ at levels ±0.01 for the $\mathrm{Re}=3.2\times10^4$ case and ±0.1 for the $\mathrm{Re}=3.5\times10^4$ case. The magnitude of $(\eta-\eta_0)$ for the $\mathrm{Re}=3.2\times10^4$ case is very small and the three-dimensional structure of the solution is barely evident in the contours of η, whereas for $\mathrm{Re}=3.5\times10^4$, the magnitude of $(\eta-\eta_0)$ is about ten times larger and its presence is clearly evident in the η contours. For the $\mathrm{Re}=3.2\times10^4$ case, the online version of the paper also provides movies showing the temporal evolution over one precession period, $\tau\approx5.5$, which is close to the rotation period of the sidewall, 2π. The isosurface movie shows that the structure precesses almost as a rotating wave. There are small structural pulsations that are partially due to the flow not having fully settled (transients are extremely long) and could also be partially due to interactions between the sidewall viscous mode and inertial waves from the interior rotating flow.

For $\mathrm{Ro}=0.50$, the critical Re for the Hopf bifurcation to the axisymmetric roll state LC_2 is about $\mathrm{Re}=3.88\times10^4$, so the three-dimensional states described above are present well below the axisymmetric Hopf bifurcation. The azimuthal wavenumber for the $\mathrm{Re}=3.2\times10^4$ case is $m=51$, and for the $\mathrm{Re}=3.5\times10^4$ case, it is $m=63$. It is reasonable for the azimuthal wavenumber to increase with Re since the thickness of the sidewall layer decreases with Re. It is very likely that at any given point in the parameter space, there are a number of such stable states with a range of m, and which one is observed as a saturated state depends on the initial conditions and is selected via an Eckhaus-type instability process. We have numerically studied such processes in rotating thermal convection, where below the onset of thermal convection throughout the entire layer, the interaction between the Coriolis force and the rotating cylinder sidewall layer leads to an instability that is confined to the sidewall boundary layer, the so-called wall modes, which, like in the present problem, have a large azimuthal wavenumber.[14] The convection problem was computationally far less demanding than the present problem, and we were able to compute the extremely slow transitions between different three-dimensional modes due to Eckhaus instabilities as the parameters were varied. Those transitions occurred over dozens of viscous times. Any attempt to conduct a similar study in the present problem, with the viscous time being of the order of Re, is prohibitively expensive computationally and impractical experimentally (one viscous time is of the order of 1 day).

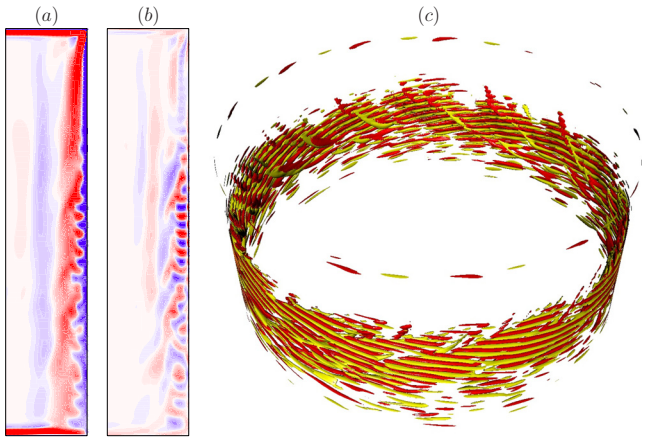

FIG. 12. (Color online) Snapshots of azimuthal vorticity η for the state at $\mathrm{Re}=4.0\times10^4$ and $\mathrm{Ro}=0.50$: contours in a partial plane $(r,z)\in[0.8,1.0]\times[0.0,1.0]$ for (a) $\eta\in[-2.0,2.0]$ and (b) $(\eta-\eta_0)\in[-2.0,2.0]$, where positive levels are red (light), negative levels are blue (dark), and zero is white, and (c) isosurfaces of $(\eta-\eta_0)$, the red (dark) isosurfaces are at level 1.0 and the yellow (light) isosurfaces are at level -1.0 (enhanced online) [URL: http://dx.doi.org/10.1063/1.3517292.8] [URL: http://dx.doi.org/10.1063/1.3517292.9] [URL: http://dx.doi.org/10.1063/1.3517292.10].

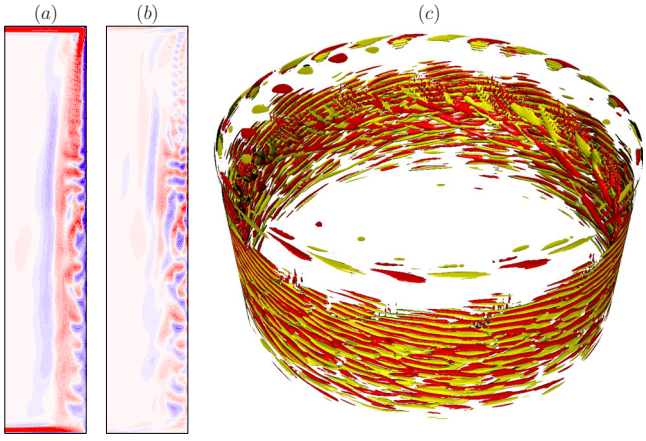

FIG. 13. (Color online) Snapshots of azimuthal vorticity η for the state at $\mathrm{Re}=5.0\times10^4$ and $\mathrm{Ro}=0.50$: contours in a partial plane $(r,z)\in[0.8,1.0]\times[0.0,1.0]$ for (a) $\eta\in[-4.0,4.0]$ and (b) $(\eta-\eta_0)\in[-4.0,4.0]$, where positive levels are red (light), negative levels are blue (dark), and zero is white, and (c) isosurfaces of $(\eta-\eta_0)$, the red (dark) isosurfaces are at level 1.0 and the yellow (light) isosurfaces are at level -1.0 (enhanced online) [URL: http://dx.doi.org/10.1063/1.3517292.11] [URL: http://dx.doi.org/10.1063/1.3517292.12] [URL: http://dx.doi.org/10.1063/1.3517292.13].

Increasing Re to 4.0×10^4 results in a very different type of three-dimensional flow. It has a number of prominent features, as illustrated in Fig. 12. From the η and $(\eta-\eta_0)$ contours near the sidewall, we find that the three-dimensional instability components are of magnitude comparable to the axisymmetric component of the flow. Different instability activities are located in regions where the LC_1 and LC_2 axisymmetric rolls were active. Note that this solution was computed for (Re,Ro) values where in the axisymmetric subspace only LC_2 is stable (i.e., in the region between the Hopf curve H_2 and the Neimark–Sacker curve NS_2). At about midheight in the sidewall layer, the perturbation azimuthal vorticity is organized into rolls with a forward tilt that precess prograde with the sidewall at a rate considerably faster than the rotation of the sidewall, about five times faster. This is consistent with the experimental observations of Hart and Kittelman.[7] Lower in the sidewall boundary layer there is also another group of forward tilted rolls, but these are less coherently organized and have some features more in common with the wavy turbulent state reported in the experiments toward the end of the ramp in Ro. Together with the various forward tilted roll structures, which are predominantly present very close to the sidewall, we see from the isosurface rendering of the flow that in the outer boundary layer there are also a number of backward tilted structures that appear to erupt from within the inner layer; their "footprints" near the sidewall are seen to periodically breakup the otherwise coherent forward tilted rolls. Finally, very close to the top corner $(r=z=1)$, there is a very localized series of small structures with azimuthal wavenumber $m=13$. From animations, we find that all of these structures are co-precessing with the dominant forward tilted rolls, and that there are slow modulations in the spatial structures, which, as in the lower Re cases, could be partially due to transient effects, or even to interactions with the inertial waves in the interior.

Further increasing Re to 5.0×10^4 (see Fig. 13), the flow state is qualitatively the same as at $\mathrm{Re}=4.0\times10^4$, but the backward tilted structures erupting from the deep inner boundary layer are much more intense and their interactions with the previously coherent forward tilted rolls have now rendered these much less coherent. The isosurface rendering has much in common visually with the Kalliroscope image of the wavy turbulent state in the experiment [see Fig. 2(d) in Ref. 7].

Reducing Ro to 0.45 so that we are in the region between H_1 and NS_1 where in the axisymmetric subspace only LC_1 is stable does not alter the qualitative nature of the three-dimensional solution (see Fig. 14). The solution at

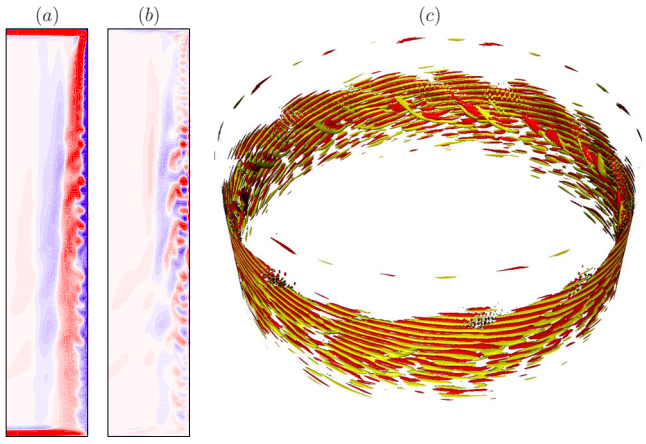

FIG. 14. (Color online) Snapshots of azimuthal vorticity η for the state at $\mathrm{Re}=5.0\times10^4$ and $\mathrm{Ro}=0.45$: contours in a partial plane $(r,z)\in[0.8,1.0]\times[0.0,1.0]$ for (a) $\eta\in[-2.0,2.0]$ and (b) $(\eta-\eta_0)\in[-2.0,2.0]$, where positive levels are red (light), negative levels are blue (dark), and zero is white, and (c) isosurfaces of $(\eta-\eta_0)$, the red (dark) isosurfaces are at level 1.0 and the yellow (light) isosurfaces are at level -1.0 (enhanced online) [URL: http://dx.doi.org/10.1063/1.3517292.14] [URL: http://dx.doi.org/10.1063/1.3517292.15] [URL: http://dx.doi.org/10.1063/1.3517292.16].

$(\mathrm{Ro},\mathrm{Re})=(0.45,5.0\times10^4)$ is very similar to that at $(\mathrm{Ro},\mathrm{Re})=(0.50,4.0\times10^4)$.

VI. DISCUSSION AND PERSPECTIVES

We have provided a comprehensive description of the basic state that is driven in a rapidly rotating cylinder by the differential corotation of the top lid. Particular attention has been given to the structure of the resulting sidewall boundary layer and its instabilities. As a consequence, we have resolved the apparent discrepancy between the experimentally observed[7] axisymmetric rolls (LC_1), which form in the upper part of the sidewall boundary layer, and the numerically observed[10] axisymmetric rolls (LC_2), which form near the bottom half of the layer. By conducting an extensive study in the (Re,Ro) parameter space, we have shown that there are two distinct axisymmetric Hopf bifurcations, each leading to one or the other of the axisymmetric roll states. The experiments were restricted by mechanical constraints on the motor, providing the basic rotation to Re values above those where the numerically observed rolls are the primary axisymmetric mode bifurcating from the basic state, while the earlier numerical study used smaller Re below where the experimentally observed rolls are the primary axisymmetric mode. We have located in this study the double Hopf bifurcation point, at $(\mathrm{Ro},\mathrm{Re})=(0.482,4.25\times10^4)$, which organizes the competition between LC_1 and LC_2 and have shown that it spawns a quasiperiodic mixed mode QP, and that further from the double Hopf point, the dynamics in the axisymmetric subspace is also complicated. The fast background rotation (large Re) not only leads to very thin boundary layers but it also allows for sustained inertial waves in the interior away from the viscous boundary layers. The two viscous sidewall modes, LC_1 and LC_2, have a very different behavior with regard to the inertial waves. The frequency associated with the roll propagation in LC_1 (high Re rolls) is too large to generate inertial waves, whereas the frequency of LC_2 does generate inertial waves, and the angle of propagation of these waves with respect to the rotation axis is as expected from the classical inviscid theory. The mixed mode, QP, and other more temporally erratic states, ET, also contain frequencies that generate inertial waves, but due to the nonperiodic nature of these states, the resultant inertial waves are rather irregular.

The fully three-dimensional simulations, however, indicate that the axisymmetric instability modes are not robust and that when the basic state becomes unstable, the nonlinearly saturated flow is three dimensional. We have found that near but below the axisymmetric Hopf bifurcations, in the (Re,Ro) parameter space, the sidewall instability consists of backward tilted diagonal rolls that precess slightly retrograde with respect to the sidewall rotation. These have high azimuthal wavenumbers ($m\approx50-70$), which vary with Re and perhaps to a lesser degree with Ro. As either Re or Ro are increased, the sidewall layer becomes unstable to more intense forward tilted diagonal rolls that precess prograde at about five times the sidewall rotation rate. This state also includes backward tilted structures that erupt from deep within the sidewall layer out to interior bulk rotating flow. Nonlinear interactions between these various boundary layer instability structures and possibly with inertial waves in the interior result in a rather complex spatiotemporal dynamics. Each of these states has been observed in the experiments of Hart and Kittelmann[7] as Ro is slowly ramped.

Inertial waves in this problem are excited by the boundary layer instabilities; this is in sharp contrast to the typical study of inertial waves in rapidly rotating systems where they are excited in a controlled fashion by external forcing. For example, McEwan[30] forced them by having the top endwall of a rapidly rotating cylinder slightly inclined away from normal to the rotation axis as well as having a slight misalignment between the rotation axis and the axis of the cylinder. Fultz[31] excited them via axial oscillations of a small disk at the center of the rotating cylinder. Manasseh,[32–34] Kobine,[35,36] and Meunier *et al.*[37,38] also forced them via precession, i.e., misalignment between the rotation axis and the axis of the cylinder. Similar inertial waves have also been generated by forced deformations of the cylinder (squeezing it between two or three external rollers).[39,40] Inertial waves generated by an instability of the Ekman layer in a precessing spheroid have also been observed numerically.[41]

Phillips[42] has a theory to suggest that there is transfer of energy between different wavenumbers following reflections from boundaries, and that for general irregular boundaries, repeated reflections can be expected to result in a statistical radiative equilibrium over the high wavenumbers, leading to a random field of inertial waves that could be regarded as a limiting condition of turbulence in a rapidly rotating fluid. In our problem, the cylinder walls are regular; however, the viscous boundary layer instabilities in some sense provide the irregular reflections for the inertial waves, leading to the type of turbulence envisioned by Phillips. The three-dimensional computed states reported on here have a strong resemblance to the wavy turbulent state in the experiments of Hart and Kittelman.[7] Further systematic investigations of the interaction between inertial waves in confined rapidly rotating flows and viscous boundary layer modes are needed; the good correspondence between our simulations and the experimental visualizations indicates that such investigations are now becoming computationally feasible.

ACKNOWLEDGMENTS

This work was supported, in part, by the U.S. National Science Foundation (Grant Nos. DMS-0505489 and DMS-0922864), the Spanish Ministry of Education and Science (Grant No. FIS2009-08821), and the Korean Science and Engineering Foundation WCU (Grant No. R32-2009-000-20021-0).

[1] J. P. Johnston, "Effects of system rotation on turbulence structure: A review relevant to turbomachinery," Int. J. Rotating Mach. **4**, 97 (1998).
[2] B. Launder, S. Poncet, and E. Serre, "Laminar, transitional, and turbulent flows in rotor-stator cavities," Annu. Rev. Fluid Mech. **42**, 229 (2010).
[3] J. E. Hart, "Sidewall instability and eddy generation in a rotating fluid subject to periodic forcing," Appl. Mech. Rev. **47**, S118 (1994).
[4] R. C. Beardsley, "A laboratory model of the wind-driven ocean circulation," J. Fluid Mech. **38**, 255 (1969).

[5]R. Krishnamurti and J. Y. Na, "Experiments in ocean circulation modelling," Geophys. Astrophys. Fluid Dyn. **11**, 13 (1978).
[6]J. Pedlosky, *Geophysical Fluid Dynamics*, 2nd ed. (Springer, New York, 1987).
[7]J. E. Hart and S. Kittelman, "Instabilities of the sidewall boundary layer in a differentially driven rotating cylinder," Phys. Fluids **8**, 692 (1996).
[8]K. Stewartson, "On almost rigid rotations," J. Fluid Mech. **3**, 17 (1957).
[9]H. Niino, "Inertial instability of the Stewartson $E^{1/4}$-layer," Fluid Dyn. Res. **3**, 407 (1988).
[10]J. M. Lopez, "Characteristics of endwall and sidewall boundary layers in a rotating cylinder with a differentially rotating endwall," J. Fluid Mech. **359**, 49 (1998).
[11]J. M. Lopez and J. Shen, "An efficient spectral-projection method for the Navier-Stokes equations in cylindrical geometries. I. Axisymmetric cases," J. Comput. Phys. **139**, 308 (1998).
[12]I. Mercader, O. Batiste, and A. Alonso, "An efficient spectral code for incompressible flows in cylindrical geometries," Comput. Fluids **39**, 215 (2010).
[13]F. Marques, I. Mercader, O. Batiste, and J. M. Lopez, "Centrifugal effects in rotating convection: Axisymmetric states and three-dimensional instabilities," J. Fluid Mech. **580**, 303 (2007).
[14]J. M. Lopez, F. Marques, I. Mercader, and O. Batiste, "Onset of convection in a moderate aspect-ratio rotating cylinder: Eckhaus-Benjamin-Feir instability," J. Fluid Mech. **590**, 187 (2007).
[15]J. M. Lopez and F. Marques, "Centrifugal effects in rotating convection: Nonlinear dynamics," J. Fluid Mech. **628**, 269 (2009).
[16]J. M. Lopez, F. Marques, A. M. Rubio, and M. Avila, "Crossflow instability of finite Bödewadt flows: Transients and spiral waves," Phys. Fluids **21**, 114107 (2009).
[17]K. Stewartson, "On the flow between two rotating coaxial disks," Proc. Cambridge Philos. Soc. **49**, 333 (1953).
[18]R. Fjortoft, "Application of integral theorems in deriving criteria of stability for laminar flows and for the baroclinic circular vortex," Geofys. Publ. **17**, 1 (1950).
[19]P. G. Drazin and W. H. Reid, *Hydrodynamic Stability*, 2nd ed. (Cambridge University Press, Cambridge, 2004).
[20]H. P. Greenspan, *The Theory of Rotating Fluids* (Cambridge University Press, Cambridge, 1968).
[21]J. Guckenheimer and P. Holmes, *Nonlinear Oscillations, Dynamical Systems, and Bifurcations of Vector Fields* (Springer, New York, 1997).
[22]Y. A. Kuznetsov, *Elements of Applied Bifurcation Theory*, 3rd ed. (Springer, New York, 2004).
[23]F. Marques, J. M. Lopez, and J. Shen, "Mode interactions in an enclosed swirling flow: A double Hopf bifurcation between azimuthal wavenumbers 0 and 2," J. Fluid Mech. **455**, 263 (2002).
[24]J. M. Lopez, J. E. Hart, F. Marques, S. Kittelman, and J. Shen, "Instability and mode interactions in a differentially-driven rotating cylinder," J. Fluid Mech. **462**, 383 (2002).
[25]F. Marques, A. Y. Gelfgat, and J. M. Lopez, "A tangent double Hopf bifurcation in a differentially rotating cylinder flow," Phys. Rev. E **68**, 016310 (2003).
[26]J. M. Lopez, Y. D. Cui, and T. T. Lim, "An experimental and numerical investigation of the competition between axisymmetric time-periodic modes in an enclosed swirling flow," Phys. Fluids **18**, 104106 (2006).
[27]J. M. Lopez and F. Marques, "Mode competition between rotating waves in a swirling flow with reflection symmetry," J. Fluid Mech. **507**, 265 (2004).
[28]J. D. Crawford and E. Knobloch, "Symmetry and symmetry-breaking bifurcations in fluid dynamics," Annu. Rev. Fluid Mech. **23**, 341 (1991).
[29]G. Iooss and M. Adelmeyer, *Topics in Bifurcation Theory and Applications*, 2nd ed. (World Scientific, Singapore, 1998).
[30]A. D. McEwan, "Inertial oscillations in a rotating fluid cylinder," J. Fluid Mech. **40**, 603 (1970).
[31]D. Fultz, "A note on overstability and the elastoid-inertia oscillations of Kelvin, Solberg, and Bjerknes," J. Atmos. Sci. **16**, 199 (1959).
[32]R. Manasseh, "Breakdown regimes of inertia waves in a precessing cylinder," J. Fluid Mech. **243**, 261 (1992).
[33]R. Manasseh, "Distortions of inertia waves in a rotating fluid cylinder forced near its fundamental mode resonance," J. Fluid Mech. **265**, 345 (1994).
[34]R. Manasseh, "Nonlinear behaviour of contained inertia waves," J. Fluid Mech. **315**, 151 (1996).
[35]J. J. Kobine, "Inertial wave dynamics in a rotating and precessing cylinder," J. Fluid Mech. **303**, 233 (1995).
[36]J. J. Kobine, "Azimuthal flow associated with inertial wave resonance in a precessing cylinder," J. Fluid Mech. **319**, 387 (1996).
[37]P. Meunier, C. Eloy, R. Lagrange, and F. Nadal, "A rotating fluid cylinder subject to weak precession," J. Fluid Mech. **599**, 405 (2008).
[38]R. Lagrange, C. Eloy, F. Nadal, and P. Meunier, "Instability of a fluid inside a precessing cylinder," Phys. Fluids **20**, 081701 (2008).
[39]C. Eloy, P. Le Gal, and S. Le Dizés, "Elliptic and triangular instabilities in rotating cylinders," J. Fluid Mech. **476**, 357 (2003).
[40]M. Le Bars, S. Le Dizés, and P. Le Gal, "Coriolis effects on the elliptic instability in cylindrical and spherical rotating containers," J. Fluid Mech. **585**, 323 (2007).
[41]J. Noir, P. Jault, and D. Cardin, "Numerical study of the motions within a slowly precessing sphere at low Ekman number," J. Fluid Mech. **437**, 283 (2001).
[42]O. M. Phillips, "Energy transfer in rotating fluids by reflection of inertial waves," Phys. Fluids **6**, 513 (1963).